Applied Catalysis A: General 417–418 (2012) 190–199

Contents lists available at SciVerse ScienceDirect

Applied Catalysis A: General

journal homepage: www.elsevier.com/locate/apcata

IR study of iridium bonded to perturbed silanol groups of Pt-HZSM5 for *n*-pentane isomerization

Herma Dina Setiabudi[a], Aishah Abdul Jalil[a], Sugeng Triwahyono[b,*], Nur Hidayatul Nazirah Kamarudin[a], Rino R. Mukti[c]

[a] Department of Chemical Engineering, Faculty of Chemical Engineering, Universiti Teknologi Malaysia, 81310 UTM Johor Bahru, Johor, Malaysia
[b] Ibnu Sina Institute for Fundamental Science Studies, Faculty of Science, Universiti Teknologi Malaysia, 81310 UTM Johor Bahru, Johor, Malaysia
[c] Division of Inorganic and Physical Chemistry, Faculty of Mathematics and Natural Science, Institut Teknologi Bandung Jl. Ganesha No. 10, Bandung, 40132, Indonesia

ARTICLE INFO

Article history:
Received 27 September 2011
Received in revised form
17 December 2011
Accepted 23 December 2011
Available online 31 December 2011

Keywords:
IrO_2
Ir/Pt-HZSM5
Perturbed silanol groups
Protonic acid sites
n-Pentane isomerization

ABSTRACT

The Ir/Pt-HZSM5 catalyst was prepared by impregnation of iridium on Pt-HZSM5. The activity of Ir/Pt-HZSM5 was tested for *n*-pentane isomerization under hydrogen stream. The introduction of iridium did not change the bands observed at 3740, 3665 and 3610 cm^{-1} indicating that neither non-acidic terminal silanol groups nor acidic bridging hydroxyl groups interacted with the iridium. Additionally, the peaks corresponding to the perturbed silanol groups at 3700 and 3520 cm^{-1} decreased significantly. X-ray photoelectron spectroscopy (XPS) analysis revealed that the iridium is in the form of IrO_2. ^{27}Al MAS NMR confirmed the elimination of distorted tetrahedral aluminum. The presence of iridium slightly increased the acidity of Pt-HZSM5 and its selectivity for iso-pentane. Hydrogen adsorption FTIR indicated that iridium enhanced the formation of protonic acid sites which may participate in the isomerization, and inhibited the formation of hydroxyl groups at 3380, 3600 and 3680 cm^{-1} which may participate in the enhancement of the cracking reaction.

1. Introduction

In recent years, bifunctional transition metal-loaded catalysts employing metal [1–6], mesoporous [7] and microporous solid oxide materials [8–12] as supports have drawn much attention due to their efficiency for isomerization of alkanes and for the synthesis of high octane gasoline. Among the available supports, zeolites appear to be promising because they are known to have a high surface area, high thermal stability and strong acidity required, for a stable, regenerable and active catalyst. Currently, zeolites are of industrial importance and contribute to the production of a majority of the world's gasoline by catalyzing the fluidized catalytic cracking (FCC) of petroleum [13].

The presence of promoters such as platinum [9,10,14], gallium [15,16] and zinc [17–19] in zeolites may favor the activity and selectivity for isomerization over the cracking activity. In particular, platinum supported on MFI-type zeolite (HZSM5) was found to be active and stable for the isomerization of *n*-alkanes [9]. The isomerization of light paraffins such as pentane, hexane and heptane proceeds due to the promotive effect of hydrogen that has migrated or spilled-over from a noble metal site onto the acidic oxide support. This catalyst behavior is referred to the hydrogen spillover effect [20]. Fujimoto et al. [9] reported that Pt/HZSM5 can enhance the selectivity for iso-pentane and decrease the formation of cracked products. The role of platinum in the H_2 spillover mechanism was confirmed by the reduction in the conversion of *n*-pentane in the absence of hydrogen, which hence allows the oligomerization reactions to occur.

The hydrogen spillover phenomenon has only been observed for a limited class of catalysts. In addition to zeolites, sulfated zirconia can also be utilized as a support and as a hydrogen spillover catalyst after being impregnated with several metals [2,21]. In certain cases, the introduction of a second metal is sometimes necessary to increase the activity of the support and suppress the production of cracked products [22,23]. In addition to platinum, gallium and zinc, iridium has been incorporated as a co-promoter to give this effect. In catalytic reforming, iridium species are well known co-promoters that are added to catalysts because of their stability during the coke removal process [24–26]. Yang and Woo [27] reported that Pt-Ir/NaY maintained better activity for the *n*-heptane reforming reaction than the Pt/NaY catalyst due to a decrease in the formation of coke. They also found that the activity for the *n*-heptane reforming reaction was enhanced over Pt-Ir/NaY. Additionally, Aboul-Gheit et al. [28] reported that Ir loaded on Pt-HZSM5 enhanced the catalytic activity for *n*-hexane hydroconversion.

* Corresponding author. Tel.: +60 7 5536076; fax: +60 7 5536080.
E-mail addresses: sugeng@utm.my, sugeng@ibnusina.utm.my (S. Triwahyono).

0926-860X/$ – see front matter © 2011 Elsevier B.V. All rights reserved.
doi:10.1016/j.apcata.2011.12.039

Although several studies have reported the importance of Ir and Pt supported on zeolite catalysts for enhancing the catalytic activity and stability, a detailed investigation of the nature of the active sites that describe the types and the strength of the interaction with molecular hydrogen, as well as its relationship to the catalytic activity have not been performed. Herein, we present an infrared (IR) spectroscopy study using iridium as a co-promoter in the Pt supported on MFI-type catalyst for the isomerization of *n*-pentane under hydrogen stream. In addition, we have studied the adsorption of hydrogen and 2,6-lutidine to elucidate the properties of surface acid sites. The presence of iridium in the Pt-HZSM5 catalyst increases the acidity of both the Lewis and protonic acid sites, decreasing the intensity of the peaks for the perturbed silanol groups at 3700 and 3520 cm^{-1} and inhibiting the formation of hydroxyl groups from molecular hydrogen at 3680, 3600 and 3380 cm^{-1}. The introduction of Ir to the Pt-HZSM5 increased the selectivity for iso-pentane and decreased the production of cracking products.

2. Experimental

2.1. Catalyst preparation

A commercial HZSM5 (Zeolyst) with Si/Al atomic ratio of 23 was used as a catalyst support. Prior to modification, HZSM5 was treated according to the method described in previous report [19]. Pt-HZSM5 was prepared by incipient wetness impregnation using aqueous solution of $H_2PtCl_6{\cdot}H_2O$ (Merck) followed by drying at 383 K overnight and calcination at 823 K for 3 h in air. The content of Pt was determined to be 0.1 wt%. Subsequently, the Ir/Pt-HZSM5 was prepared by incipient wetness impregnation of Pt/HZSM5 with aqueous solution of $IrCl_3{\cdot}3H_2O$ (Merck) followed by drying at 383 K overnight and calcination at 823 K for 3 h in air. The content of Ir was determined to be 0.1 wt%.

2.2. Catalyst characterization

X-ray photoelectron spectroscopy (XPS) analysis of Ir/Pt-HZSM5 was conducted on a Kratos Ultra spectrometer with MgKα radiation source (10 mA, 15 kV). The XPS peaks are internally referenced to the binding energy of C (1s) peak at 284.5 ± 0.1 eV.

^{27}Al MAS NMR and ^{29}Si MAS NMR spectra were recorded on a Bruker Avance 400 MHz 9.4 T spectrometer at frequency of 104.2 MHz and 79.4 MHz, respectively. The ^{27}Al MAS NMR spectra were obtained using pulse length of 1.9 μs, spin rate of 7 kHz and relaxation time delay of 2 s. The ^{29}Si MAS NMR spectra were recorded using 4 μs radio frequency pulses, a recycle delay of 60 s and spinning rate of 7 kHz using a 4 mm zirconia sample rotor.

The crystalline structure of the catalyst was confirmed by X-ray diffraction (XRD) recorded on a powder diffractometer (40 kV, 40 mA) using Cu Kα radiation source. The BET specific surface area was calculated from the adsorption data of N_2 adsorption–desorption isotherm in the relative pressure of 0.01–0.2. The isotherm was measured on a Quantachrome Autosorb-1 instrument in which the sample was outgassed at 573 K for 3 h prior to the analysis.

Fourier Transform Infra Red (FTIR) measurements were carried out with Perkin–Elmer Spectrum GX FT-IR Spectrometer. Before the analysis, catalysts were activated according to the method described in the literature [29]. In brief, a self-supported wafer placed in an in-situ stainless steel IR cell with CaF_2 windows was heated at 673 K in hydrogen flow for 3 h and outgassed at 673 K for 3 h. The FTIR spectra were recorded at room temperature. Hydrogen adsorption on activated Pt-HZSM5 and Ir/Pt-HZSM5 catalysts were performed to observe the interaction of molecular and/or atomic hydrogen with the surface of catalysts. The activated catalysts were cooled to 173 K and held at this temperature for 15 min. 13.3 kPa of hydrogen was then dosed to the catalyst, followed by stepwise heating from 173 K to 573 K. The heating was held for 15 min at each temperature.

2,6-lutidine basic probe molecule was used to evaluate the acidity of catalysts. 2,6-lutidine pre-adsorbed catalyst was prepared as follows. The activated catalyst was exposed to 2 Torr of 2,6-lutidine at room temperature for 30 min, followed by outgassing at room temperature, 373 and 473 K for 30 min, respectively. The spectra were recorded at room temperature.

For the observation of the generation of protonic acid sites from molecular hydrogen on the catalysts, the 2,6-lutidine preadsorbed catalyst was exposed to 13.33 kPa of hydrogen at room temperature. Then, the catalyst was heated up stepwise from room temperature to 473 K in 50 K increments. The spectra were recorded at room temperature.

In order to directly compare the surface coverage of all spectra, the overtone and combination vibration of the MFI between 2100 and 1550 cm^{-1} after activation were used [30].

2.3. Isomerization of n-pentane

Isomerization of *n*-pentane was carried out on a microcatalytic pulse reactor at 573 K under the hydrogen stream. Prior to the isomerization, 0.2 g of catalyst was activated in oxygen stream (F_{Oxygen} = 100 ml/min) for 1 h followed by hydrogen stream ($F_{Hydrogen}$ = 100 ml/min) for 3 h at 673 K and cooled down to 573 K in a hydrogen stream as described in previous report [31]. A dose of *n*-pentane (43 μmol) was passed over the activated catalyst and the products were trapped at 77 K before being flash-evaporated into an online 6090N Agilent Gas Chromatograph equipped with HP-5 Capillary Column and FID detector. The intervals between doses were kept constant at 20 min.

The selectivity to particular product (S_i) was calculated according to Eq. (1)

$$S_i = \frac{A_i}{\sum A_i - A_{n\text{-pentane}}} \times 100 \quad (1)$$

where A_i and $A_{n\text{-pentane}}$ are corrected chromatographic area for particular compound and for residual *n*-pentane. The conversion of *n*-pentane ($X_{n\text{-pentane}}$) was determined by Eq. (2)

$$X_{n\text{-pentane}} = \frac{\sum A_i - A_{n\text{-pentane}}}{\sum A_i} \times 100. \quad (2)$$

3. Results and discussion

3.1. Structural properties of catalysts

Fig. 1 shows the XPS Ir 4f spectrum of Ir/Pt-HZSM5. In general, $4f_{7/2}$ core level for metallic Ir appears at 60–61 eV, while that for the oxidized Ir appears at higher energies [32]. The doublet with binding energies of 61.4 ($Ir4f_{7/2}$) and 64.2 eV ($Ir4f_{5/2}$) is thus assigned to Ir^{4+}, possibly as IrO_2. The presence of Ir^{4+}, possibly as IrO_2 was also observed in Ir/SiO_2 and Ir/Al_2O_3 catalysts reported by Burkhard and Schmidt [33]. In contrast, these results were inconsistent with Voskobojnikov et al. [34] for the Ir-HZSM5 catalyst prepared by ion exchange of the HZSM5 with an aqueous solution of the $[Ir(NH_3)_5H_2O]^{3+}$ complex in which only the Ir^{3+} was observed in the XPS Ir 4f spectra. They reported that the Ir-HZSM5 was not subject to any treatment in air at elevated temperatures, and thus the formation of Ir^{4+} is very unlikely.

^{27}Al MAS NMR and ^{29}Si MAS NMR experiments were carried out to examine the effect of iridium on the chemical environments of the aluminum and silicon atoms of the corresponding samples, and

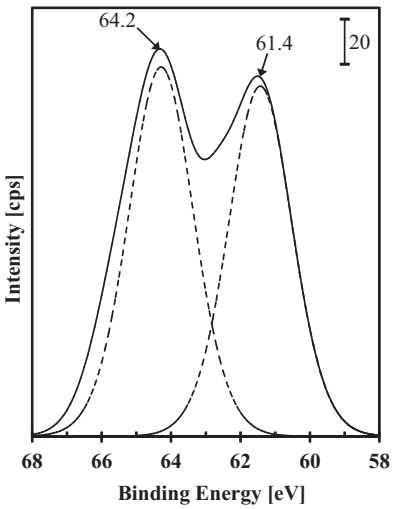

Fig. 1. XPS spectrum of the Ir 4f line for the Ir/Pt-HZSM5.

the results are shown in Fig. 2. Fig. 2(A) shows the ^{27}Al MAS NMR spectra of the Pt-HZSM5 and Ir/Pt-HZSM5 catalysts. The spectrum of Pt-HZSM5 shows three signals at 64, 55 and 0 ppm corresponding to the distorted tetrahedral sites, tetrahedral aluminum in the framework structure and octahedrally coordinated extraframework aluminums, respectively [35]. However, only two signals at 55 and 0 ppm were observed in the ^{27}Al MAS NMR spectrum for Ir/Pt-HZSM5, and no peaks corresponding to distorted tetrahedral sites were observed. In addition, the intensity of the peak corresponding to the octahedrally coordinated extraframework aluminums increased slightly after the introduction of iridium. This result suggests that the presence of iridium could stabilize the MFI framework structure by eliminating the distorted tetrahedral sites caused by the presence of platinum. The stabilizing effect of the metal on the MFI framework structure was also observed for Pd loaded Cu/HZSM5 as reported by Praserthdram et al. [36]. They found that the presence of Pd (approximately 0.3 wt%) caused the elimination of the signal related to the octahedral aluminum and only one signal in the ^{27}Al MAS NMR spectrum was observed at approximately 50 ppm. They suggested that the introduction of 0.3 wt% Pd stabilized the MFI framework by preventing the occurrence of dealumination.

The ^{29}Si MAS NMR spectra of the Pt-HZSM5 and Ir/Pt-HZSM5 catalysts are shown in Fig. 2(B). The spectra for both catalysts are similar to those reported previously for ZSM-5 zeolites [37,38]. For Pt-HZSM5, the dominant signal at approximately −112.8 ppm is assigned to $(\equiv SiO)_4Si$ while the shoulder signal between −103 and −108 ppm corresponded to $(\equiv SiO)_3Si$ in the HZSM5 framework [39]. Additionally, a small shoulder signal in the range between −120 and −135 ppm may be attributed to the existence of crystallographically inequivalent sites in the Pt-HZSM5 catalyst [40]. For Ir/Pt-HZSM5, the introduction of iridium on Pt-HZSM5 developed a new shoulder in the range between −90 and −103 ppm, and eliminated the shoulder in the range between −120 and −135 ppm. This result indicates the formation of $(\equiv SiO)_2Si$ sites by eliminating the crystallographically inequivalent sites in Pt-HZSM5 catalyst. The elimination of crystallographically inequivalent sites may be related to the elimination of distorted tetrahedral aluminum sites caused by the interaction of iridium with perturbed silanol groups of Pt-HZSM5 catalyst. However, these changes only caused small effect on the chemical environment of silicon atoms and not in a stage to destroy the silicate framework of Pt-HZSM5. A similar phenomenon was reported by Ma et al. [41] where the presence of Mo did not destroy the silicate framework of HMCM-22. They found no distinct difference between the ^{29}Si MAS NMR spectra for 10Mo/HMCM-22 and the parent HMCM-22. They suggested that although the molybdenum species have a strong interaction with the framework of HMCM-22, they do not destroy or change the silicate framework.

XRD patterns of Pt-HZSM5 and Ir/Pt-HZSM5 are shown in Fig. 3. The peaks in the range of $2\theta = 7–10^\circ$ and $22–25^\circ$ were identified as reflections from the HZSM5 zeolite [42–44]. The introduction of iridium did not change the peak position for Pt-HZSM5 at $2\theta = 7–10^\circ$ and $22–25^\circ$ but slightly increased the intensity of the peaks and the crystallinity of Pt-HZSM5 due to the elimination of distorted aluminum sites. These results also indicated that the iridium may interact with structural or lattice defect sites stabilizing the crystalline structure of Pt-HZSM5 and leading to a more ordered framework structure. In addition, the absence of peaks at $2\theta = 39.7^\circ$, 46.2°, 40.7° and 47.3° ascribed to Pt(1 1 1), Pt(2 0 0), Ir(1 1 1) and Ir(2 0 0), respectively [45,46], may be due to very small amounts of

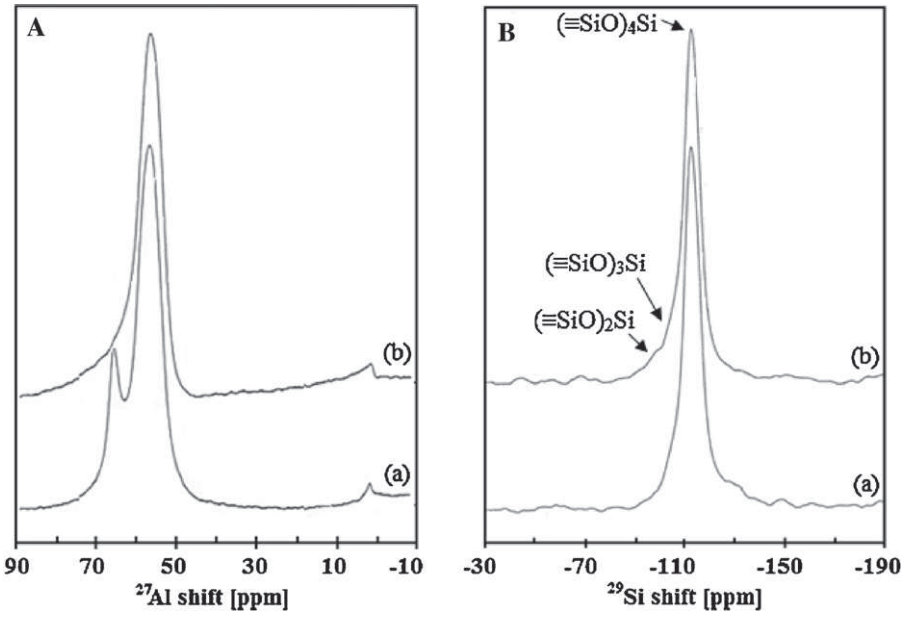

Fig. 2. (A) ^{27}Al MAS NMR (B) ^{29}Si MAS NMR spectra of (a) Pt-HZSM5 and (b) Ir/Pt-HZSM5.

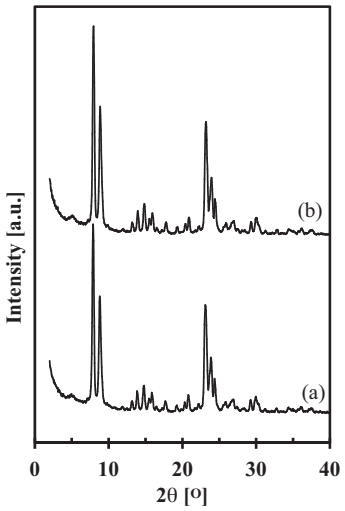

Fig. 3. XRD patterns of (a) Pt-HZSM5 and (b) Ir/Pt-HZSM5.

Pt and iridium species that are undetectable with XRD. The absence of peaks may also be attributed to the crystallinities of Pt and iridium species providing a poor comparison with the HZSM5 support. An increase in the crystallinity of the support caused by the introduction of the metal was observed for the magnesium loaded dealuminated β zeolite reported by Li et al. [47]. The increasing of magnesium loading caused a notable increase in the intensity of the most significant diffraction peaks. They suggested that magnesium ions occupy silanol nests or other structural defect sites stabilizing the crystalline structure and increasing the intensity of the most significant lines in the XRD pattern.

The physical analysis of the nitrogen adsorption–desorption isotherm showed that the presence of iridium in Pt-HZSM5 increased the BET specific surface area from 444 to 463 $m^2\,g^{-1}$ due to the increase (approximately 13.3%) in the crystallinity of Pt-HZSM5 at $2\theta = 7–10^\circ$. This result is inconsistent with the work by Aboul-Gheit et al. in which the introduction of 0.35 wt% platinum and 0.35 wt% iridium to HZSM5 decreased the specific surface area of the catalyst [28]. The decrease in the surface area may be caused by the blockage of a portion of the micropores in the support with Pt or Ir species.

Fig. 4 shows the IR spectra of the activated Pt-HZSM5 and Ir/Pt-HZSM5 catalysts in the region between 3800 and 1400 cm^{-1}. The region between 2100 and 1500 cm^{-1} is attributed to the vibrational

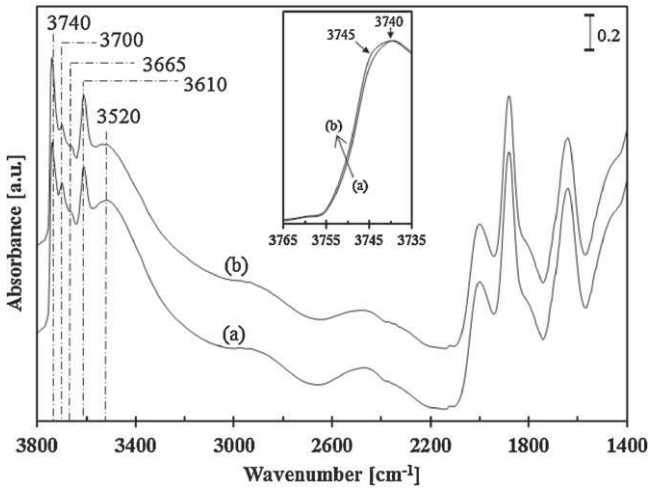

Fig. 4. IR spectra of activated (a) Pt-HZSM5 and (b) Ir/Pt-HZSM5.

overtones of the stretching and bending modes of T–O units, and the region between 3800 and 3500 cm^{-1} is related to the vibrational hydroxyl groups. The vibrations of the MFI in the Pt-HZSM5 catalyst are similar to that observed for the Ir/Pt-HZSM5 catalyst, which indicated that the introduction of iridium did not change the lattice structure of the HZSM5 support. In the OH stretching region, five bands were observed for both samples. They included a narrow band at 3740 cm^{-1} with two shoulder bands at 3700 and 3665 cm^{-1}, a much weaker band at 3610 cm^{-1} and a broad weak absorption band centered near 3520 cm^{-1}. The band at 3740 cm^{-1} is assigned to the non-acidic terminal silanol groups (Si—OH) located on the external surface of the zeolite. A band at 3610 cm^{-1} and a shoulder band at 3665 cm^{-1} are assigned to the Brönsted OH band associated with bridging hydroxyl groups (Si(OH)Al) located inside the zeolite structure and the extraframework Al—OH species resulting from limited hydrothermal degradation during the calcination process [48], respectively. The weak band at 3700 cm^{-1} and the broad band at 3520 cm^{-1} may be associated with the perturbation of OH groups through the surrounding by lattice defects or extra-lattice oxygen [49]. The presence of iridium did not alter the intensities of the bands at 3740, 3665 and 3610 cm^{-1} indicating neither non-acidic terminal silanol groups nor acidic bridging hydroxyl groups (Si(OH)Al) interacted with the iridium. However, the band corresponding to non-acidic terminal silanol groups at 3740 cm^{-1} broadened to higher wavenumber around 3745 cm^{-1} after the introduction of iridium. In addition, the intensities of the bands associated with the perturbed silanol groups at 3700 and 3520 cm^{-1} decreased slightly with the addition of iridium. These may be related to the formation of non-acidic geminal silanol groups at 3745 cm^{-1} by interaction of iridium with perturbed silanol groups of Pt-HZSM-5.

The change in the structure of HZSM5 caused by metal exchange was observed in Ir-exchanged HZSM5 as reported by Mihaylov et al. [50]. The sample was prepared by solid-state ion exchange of HZSM5 with an aqueous solution of $IrCl_3{\cdot}3H_2O$ followed by heating in a dry Ar flux (40 ml/min) at 723 K for 5 h. The IR spectra indicated the presence of Ir on HZSM5 leading to a decrease in the intensity of the band at 3610 cm^{-1}, which was due to partial exchange of isolated acidic hydroxyl groups with iridium cations. There was no change in the band at 3740 cm^{-1} indicating that the non-acidic terminal silanol groups did not interact with the iridium. A similar result using Zn ions-exchanged HZSM5 was also reported by Kazansky et al. [51] and Biscardi et al. [18]. Kazanzky et al. reported that an increase in the amount of zinc ions increased the number of substitutions of the acidic hydroxyl groups with zinc ions. The effect of Pt species on the OH groups of HZSM5 has been reported by Babůrek and Nováková in which Pt-HZSM5 was prepared by ion exchange using $Pt(NH_3)_4Cl_2$ and an NH_4-ZSM-5 solution [52]. The IR spectra showed that the presence of Pt did not change the terminal silanol groups at 3746 cm^{-1} or the bridging hydroxyl groups at 3610 cm^{-1}. These results indicated that the Pt did not interact with the non-acidic terminal silanol groups or the acidic bridged hydroxyl groups in the HZSM5, which is consistent with the results obtained for the Pt-HZSM5 and Ir/Pt-HZSM5 catalysts in this study.

Fig. 5 shows the IR spectra for the adsorption of hydrogen on activated Pt-HZSM5 and Ir/Pt-HZSM5 catalysts as the temperature was varied from 273 K to 573 K. The presence of iridium was responsible for the dual absorption bands at 2925 and 2855 cm^{-1} indicating the presence of the polarizing interaction between iridium and the perturbed silanol groups through the extra-lattice oxygen in Pt-HZSM5. However, these bands were not observed on Pt-HZSM5 indicating that the Pt did not interact with any of the silanol or hydroxyl groups or the framework of HZSM5. Dual absorption band in the range of 2500–3000 cm^{-1} has been observed on metal exchange zeolites including Rb or Na exchanged zeolite X, which are used in methanol adsorption studies [53].

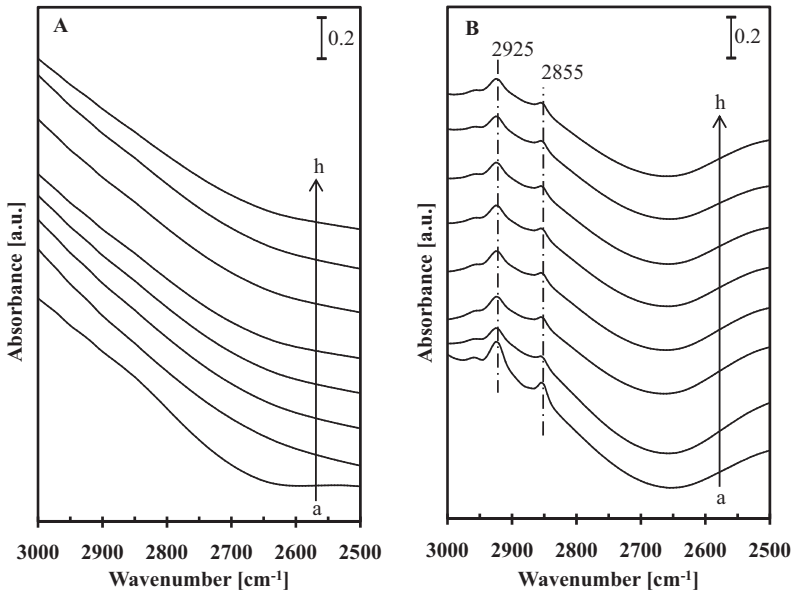

Fig. 5. IR spectra of hydrogen adsorbed on activated (A) Pt-HZSM5 and (B) Ir/Pt-HZSM5 when the catalysts were exposed to 13.3 kPa hydrogen at 173 K, followed by heating at (a) 273 K, (b) 303 K, (c) 323 K, (d) 373 K, (e) 423 K, (f) 473 K, (g) 523 K and (h) 573 K.

The changes in the hydroxyl vibration region caused by adsorption of molecular hydrogen for the temperature range of 173–573 K are shown in Fig. 6. The adsorption of molecular hydrogen on the Pt-HZSM5 catalyst at 173 K strongly altered the OH stretching band of the acidic bridging hydroxyl groups at 3610 cm^{-1} and intensified the band at 3700 cm^{-1}. In addition, a new broad band centered below 3500 cm^{-1} has appeared (Fig. 6A). An increase in the adsorption temperature to 223 K intensified the band at 3700 cm^{-1} due to an increase in the amount of adsorbed molecular hydrogen. At 248 K, the band at 3700 cm^{-1} has been partially eliminated, and new broad bands at 3680 and 3600 cm^{-1} have appeared. In addition, the broad band centered below 3500 cm^{-1} has shifted to a lower frequency (3380 cm^{-1}). Further heating to 573 K caused the bands of the perturbed silanol groups at 3700 and 3520 cm^{-1} to disappear, and the bands at 3690, 3675, 3600 and 3380 cm^{-1} to intensify. In contrast, the intensity of the band at 3740 cm^{-1} did not change with the adsorption of hydrogen species. This revealed that non-acidic terminal silanol (Si—OH) groups did not interact with molecular and atomic hydrogen in the temperature range of 173–573 K under the given experimental conditions.

Elimination of the bands at 3700, 3610 and 3520 cm^{-1} and the development of new bands at 3690, 3675, 3600 and 3380 cm^{-1} caused by raising the adsorption temperature indicated that the adsorbed hydrogen species exhibit different characteristics as the temperature was varied. The adsorbed molecular hydrogen at 223 K and below most likely began to dissociate into atomic hydrogen species on the Pt-HZSM5 catalyst at 248 K. The peaks at 3700, 3610 and 3520 cm^{-1} shifted to lower frequencies at 3680, 3600 and 3380 cm^{-1}, respectively, due to the presence of atomic hydrogen bonding interactions.

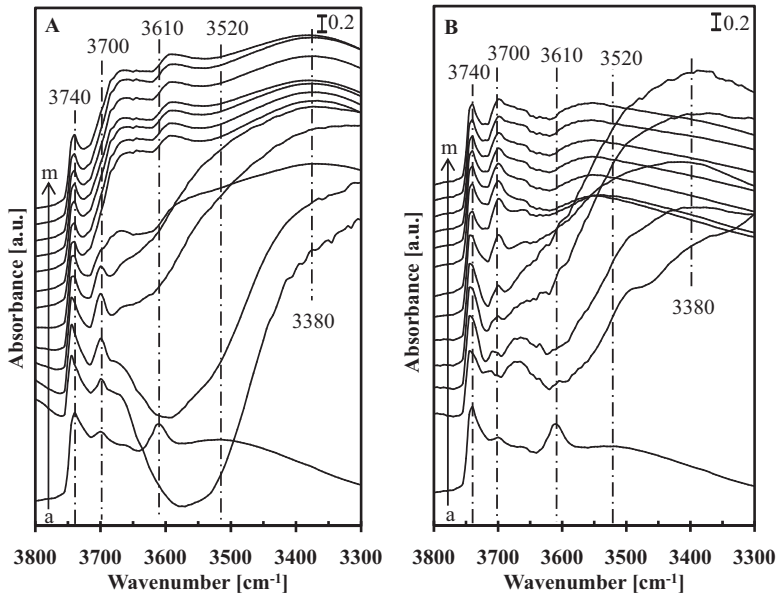

Fig. 6. IR spectra of hydrogen adsorbed on activated (A) Pt-HZSM5 and (B) Ir/Pt-HZSM5 when the catalysts were exposed to 13.3 kPa hydrogen at (b) 173 K, followed by heating at (c) 198 K, (d) 223 K, (e) 248 K, (f) 273 K, (g) 303 K, (h) 323 K, (i) 373 K, (j) 423 K, (k) 473 K, (l) 523 K and (m) 573 K. (a) Before exposure to hydrogen.

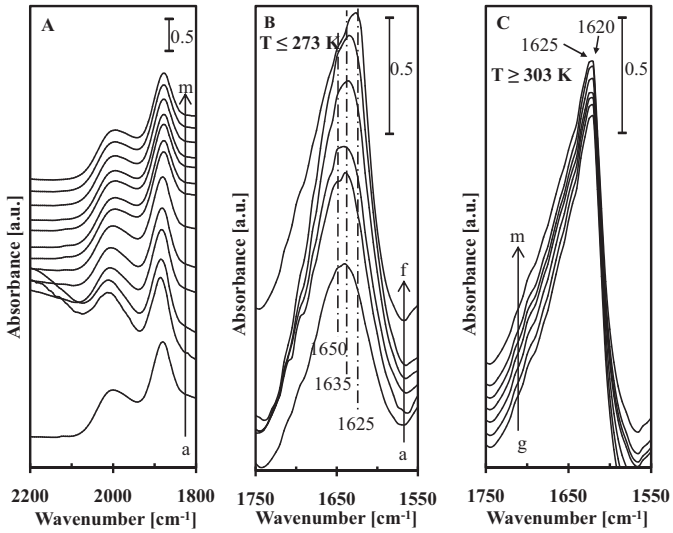

Fig. 7. IR spectra of hydrogen adsorbed on activated Pt-HZSM5 when the catalyst was exposed to 13.3 kPa hydrogen at (b) 173 K, followed by heating at (c) 198 K, (d) 223 K, (e) 248 K, (f) 273 K, (g) 303 K, (h) 323 K, (i) 373 K, (j) 423 K, (k) 473 K, (l) 523 K and (m) 573 K. (a) Before exposure to hydrogen. (A) Vibrational lattice stretching frequency in the region of 2200–1800 cm^{-1}; (B) vibrational lattice stretching frequency in the region of 1750–1550 cm^{-1} at 273 K and below; (C) vibrational lattice stretching frequency in the region of 1750–1550 cm^{-1} at 303 K and above.

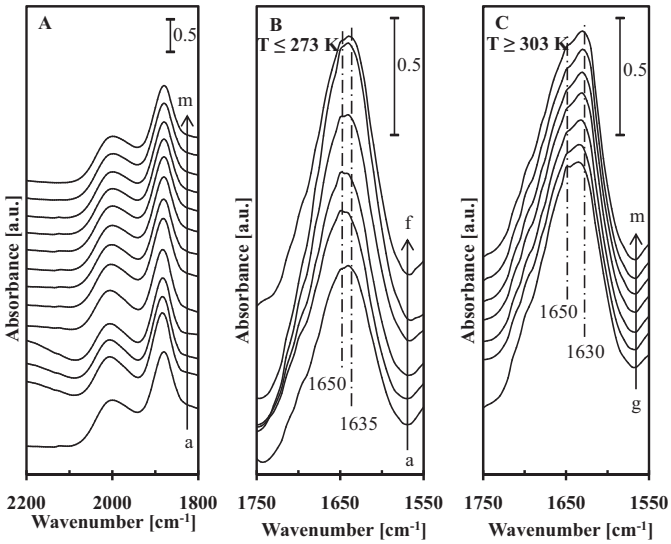

Fig. 8. IR spectra of hydrogen adsorbed on activated Ir/Pt-HZSM5 when the catalyst was exposed to 13.3 kPa of hydrogen at (b) 173 K, followed by heating at (c) 198 K, (d) 223 K, (e) 248 K, (f) 273 K, (g) 303 K, (h) 323 K, (i) 373 K, (j) 423 K, (k) 473 K, (l) 523 K and (m) 573 K. (a) Before exposure to hydrogen. (A) Vibrational lattice stretching frequency in the region of 2200–1800 cm^{-1}; (B) vibrational lattice stretching frequency in the region of 1750–1550 cm^{-1} at 273 K and below; (C) vibrational lattice stretching frequency in the region of 1750–1550 cm^{-1} at 303 K and above.

The result of molecular hydrogen adsorption on the Ir/Pt-HZSM5 catalyst is shown in Fig. 6(B) and is similar to that of the Pt-HZSM5 catalyst in Fig. 6(A). For the adsorption of hydrogen on the Ir/Pt-HZSM5 catalyst at 223 K and below, the intensities of the bands at 3700 cm^{-1} shifted to 3705 cm^{-1} due to the interaction of the surface with the physically adsorbed molecular hydrogen. In addition, the band for the acidic hydroxyl groups at 3610 cm^{-1} was strongly altered. At 248 K and above, the band at 3705 cm^{-1} disappeared, and the band at 3700 cm^{-1} was restored and intensified. Similar with the results obtained for Pt-HZSM5, the intensity of the band at 3740 cm^{-1} did not change with the adsorption of hydrogen species for all of the adsorption temperatures studied. The differences between Pt-HZSM5 and Ir/Pt-HZSM5 were observed in the adsorption at 273 K and above. By heating the Ir/Pt-HZSM5 catalyst to 273 K and above in the presence of molecular hydrogen, the absorbance band at 3700 cm^{-1}, which may be attributed to the atomic hydrogen-bonding with $Si(OH)IrO_2$ did not change, and the band ascribed to molecular hydrogen interactions that was centered at 3380 cm^{-1} disappeared. Simultaneously, a broad band centered at 3560 cm^{-1} was observed. The band at 3560 cm^{-1} is probably a superposition of the atomic hydrogen bonding interactions with the bridged hydroxyl groups and a new band arising from the hydrogen perturbed by the addition of iridium. The results strongly suggested that the hydrogen bonding interactions at 3680, 3600 and 3380 cm^{-1} were not observed due to the perturbed silanol groups being occupied by iridium.

The change in the absorbance bands caused by the adsorption of molecular hydrogen was also observed for the vibrational lattice stretching frequency in the region of 2200–1550 cm^{-1} for both the Pt-HZSM5 (Fig. 7) and the Ir/Pt-HZSM5 (Fig. 8) catalysts. At low temperatures, the bands at 1650 and 1635 cm^{-1} were observed for both catalysts and are due to the adsorption of molecular hydrogen. For Pt-HZSM5, an increase in the temperature shifted the bands at 1650 and 1635 cm^{-1} to 1625 and 1620 cm^{-1}, respectively, due to the presence of atomic hydrogen bonding interactions with perturbed silanol groups. In addition, the changes in the absorbance bands at 3700 and 3520 cm^{-1} were induced by adsorbed hydrogen species. However, no significant change was observed for the vibrational lattice stretching frequency in the region of 2200–1750 cm^{-1} indicating that there is no interaction between adsorbed hydrogen species with the non-acidic terminal silanol (SiOH) groups.

A similar result was observed for the adsorption of molecular hydrogen on the Ir/Pt-HZSM5 catalyst (Fig. 8) at low temperatures. Similar with the result obtained for Pt-HZSM5, no change was observed on the vibrational lattice stretching frequency in the region of 2200–1750 cm^{-1} for Ir/Pt-HZSM5. The absorbance band at 1650 cm^{-1} slightly intensified at 243 K and below indicating adsorption of molecular hydrogen on $Si(OH)IrO_2$ as well as the band at 3700 cm^{-1} shifted to 3705 cm^{-1}. At 273 K, the bands at 1650 and 1635 cm^{-1} did not vary significantly. However, the band at 1635 cm^{-1} shifted approximately 5 cm^{-1} to 1630 cm^{-1} and intensified as the catalyst was heated above 273 K. The IR bands centered at 1650 and 1635 cm^{-1} revealed the presence of hydrogen bonding interaction with $Si(OH)IrO_2$ and these bands supported the inhibition of adsorbed atomic hydrogen at 1625 cm^{-1}.

DRIFT studies on the adsorption of molecular hydrogen on ZSM-5 based catalysts were performed by Kazansky et al. [51,54]. For the adsorption of molecular hydrogen at 77 K, stretching bands attributed to adsorbed molecular hydrogen were observed at 3930–3950 and 4005 cm^{-1}. The intensity of the band attributed to molecular hydrogen adsorption at 3935 cm^{-1} shifted to a lower stretching frequency (1934 cm^{-1}) at room temperature and above. This shift is attributed to hydrogen-bonding with basic oxygen to produce an acidic hydroxyl band at 3610 cm^{-1}. This result indicated that the dissociative adsorption of molecular hydrogen on Zn-ZSM5 occurs through an acid–base pairs, which consisted of a positively charged zinc cation and a negatively charged basic oxygen atom. We have reported dissociative adsorptions of molecular hydrogen and alkanes on PSZ [19], PWZ [55,56] and Zn-HZSM5 [19] catalysts at relatively high temperatures as evidenced by pyridine preadsorbed FTIR spectroscopy. The atomic hydrogen was formed as a protonic acid site when the catalysts were heated under molecular hydrogen or *n*-pentane in the gas phase. The formation of atomic hydrogen as protonic acid sites was also confirmed by the formation of H–D when the catalyst was heated under a mixture of hydrogen and deuterium [55]. Kazansky et al. reported the heterolytic dissociative adsorption of hydrogen on Zn loaded HZSM5 to form a

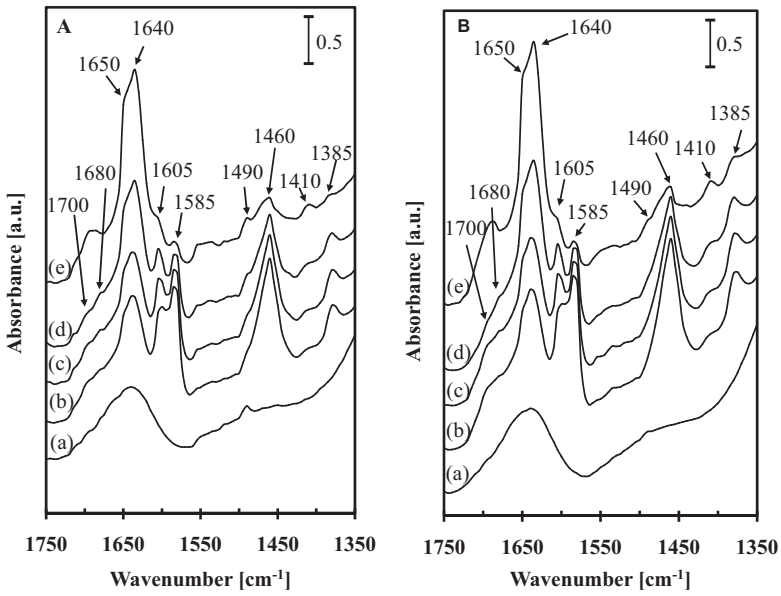

Fig. 9. IR spectra of 2,6-lutidine adsorbed on activated (A) Pt-HZSM5 and (B) Ir/Pt-HZSM5 at (b) room temperature, followed by heating in a vacuum at (c) room temperature, (d) 373 K, (e) 473 K. (a) Before exposure to 2,6-lutidine.

protonic acid site and a hydride, which perturbed the acid–base Zn^{+2}–O^{-2} pairs in the ZnHZSM5 [51].

3.2. Nature and strength of acidity

In general, the introduction of iridium will influence the acidic character of the sample. The nature of acid sites in the Pt-HZSM5 and Ir/Pt-HZSM5 catalysts was qualitatively probed by 2,6-lutidine adsorption monitored by IR spectroscopy. 2,6-lutidine ($pK_b = 7.4$) is more basic than pyridine ($pK_b = 8.8$) and is used to study the relatively weak Brönsted acid sites and the acidic centers of Lewis acid sites [57]. Fig. 9 shows the IR spectra of adsorbed 2,6-lutidine on the activated Pt-HZSM5 (A) and Ir/Pt-HZSM5 (B) catalysts in the region of 1750–1350 cm^{-1} as a function of outgassing temperature. The 2,6-lutidine pre-adsorbed catalysts were outgassed at room temperature, 373 K and 473 K. Both catalysts showed several absorption bands at 1700, 1680, 1650, and 1640 cm^{-1}, which are associated with the 2,6-lutidinium cations adsorbed on Brönsted acid sites. The absorbance bands at 1605, 1585, 1490, 1460, 1410 and 1385 cm^{-1} corresponded to the Lewis acid region [58,59].

Based on literature data for 2,6-lutidine adsorption, the bands in this experiment can be summarized as follows [59,60]:

(i) For the Brönsted acid region, strong doublet bands at 1650 and 1640 cm^{-1} observed for both samples can be assigned to the 8a and 8b mode of protonated 2,6-lutidine adsorbed on Brönsted acid sites. In addition to the strong doublet bands, a weak doublet band at 1700 and 1680 cm^{-1} is due to the 8a and 8b mode of lutidinium cations adsorbed on Brönsted acid sites.
(ii) For the Lewis acid region, the doublet band located at 1605 and 1585 cm^{-1} can be associated to the 8a and 8b mode of the coordinated or H-bonded 2,6-lutidine to the surface OH groups. A second doublet band assigned to the 19a and 19b mode of both liquid-like (physisorbed) and H-bonded 2,6-lutidine species was observed at 1490 and 1410 cm^{-1}. In addition, a third doublet band was observed at 1460 and 1385 cm^{-1}, and is due to the asymmetric and symmetric of δ_{CH_3} deformation modes.

For both catalysts, 2,6-lutidine probe molecules were able to interact strongly with acidic sites at room temperature and were retained at the outgassing temperature of 473 K. The changes in the acid sites are more clearly illustrated in Fig. 10 in which the absorbance of IR bands at Brönsted acid sites (1650 and 1640 cm^{-1}) and Lewis acid sites (1605 and 1585 cm^{-1}) for Pt-HZSM5 (Fig. 10A) and Ir/Pt-HZSM5 (Fig. 10B) was plotted as a function of the outgassing temperatures. A high outgassing temperature led to a higher concentration of lutidinium cations on Brönsted acid sites and a lower concentration of 2,6-lutidine adsorbed on Lewis acid sites. The increase in the absorbance bands ascribed to the Brönsted acid sites at higher outgassing temperatures may be related to the steric shielding of the methyl group in which the removal of 2,6-lutidine adsorbed on the Lewis acid sites allows the lutidinium cations to access relatively weaker protonic acid sites inside the zeolite bulk. Both catalysts possessed a considerable number of relatively weak and medium acid sites as well as strong Brönsted and Lewis acid sites. Generally, the presence of iridium in the sample slightly increased the intensity of the bands associated with the Brönsted and Lewis acid sites due to the interaction between iridium and lattice defects or extra-lattice oxygen. This result is similar with our recent publication [31], in which the introduction of iridium species influenced the acidic properties of HZSM5 as well as the generation of small amount of protonic and Lewis acid sites, which may be due to the interaction between iridium and lattice defects or extra-lattice oxygen.

The trend observed for both the Pt-HZSM5 and Ir/Pt-HZSM5 is similar to the result observed for the HZSM5 zeolite reported by Armaroli et al. [58], even though there are some differences in the acidity of the samples. The bands associated with 2,6-lutidine adsorbed on Lewis acid sites nearly disappeared at 393 K for the HZSM5 samples but these bands were still retained in the outgassing at 473 K and below for both the Pt-HZSM5 and Ir/Pt-HZSM5 catalysts in this experiment. The nature of the acidic sites on Pt-HZSM5 and Ir/Pt-HZSM5 is different in comparison to metal-exchanged zeolitic materials or mesoporous materials. Li et al. [61] found that the addition of iridium to HZSM5 showed a dramatic negative effect on the Brönsted and Lewis acid sites. During the impregnation of HZSM5 with an aqueous solution of $H_2IrCl_6{\cdot}H_2O$ followed by calcination, HCl was formed and led to dealumination of the HZSM5 zeolite. Hence, severe loss of Brönsted and Lewis acid sites was observed. In previous work, we reported that the preparation of ZnHZSM5 by impregnation of the HZSM5 with a nano-Zn^{2+}/N,N-dimethylformamide solution eliminated weak and

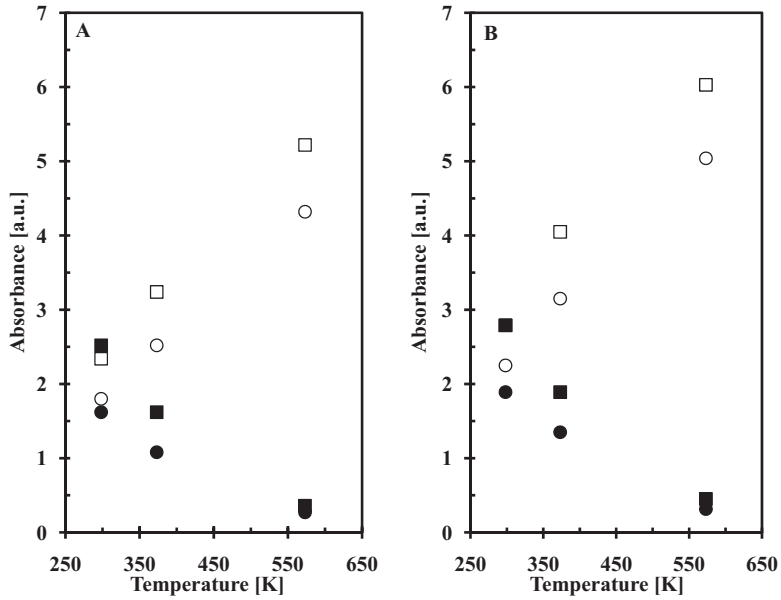

Fig. 10. Absorbance of IR bands at Brönsted and Lewis acid sites of (A) Pt-HZSM5 and (B) Ir/Pt-HZSM5 after removal of 2,6-lutidine at different temperatures. (○) Brönsted acid sites at 1650 cm^{-1}; (□) Brönsted acid sites at 1640 cm^{-1}; (●) Lewis acid sites at 1605 cm^{-1}; (■) Lewis acid sites at 1585 cm^{-1}.

medium protonic acid sites and generated a significant number of strong Lewis acid sites [19]. The conversion of relatively weak and medium protonic acid sites to strong Lewis acid sites on HZSM5 by the addition of a metal oxide was also reported by Mao et al. [62] in which MgO/HZSM5 prepared by incipient wetness impregnation of HZSM5 with an aqueous solution $Mg(NO_3)_2$, possesses a significant number of weak and strong protonic and Lewis acid sites. Generally, the elimination of protonic acid sites and the development of strong Lewis acid sites on HZSM5 may be caused by the existence of metal species bonded to the non-acidic terminal silanol (SiOH) groups and/or the bridging hydroxyl (SiOHAl) groups on the surface of HZSM5.

3.3. Hydrogen molecule-originated protonic acid sites

Fig. 11(A) shows the changes in the IR spectra when the 2,6-lutidine preadsorbed activated Pt-HZSM5 catalyst was heated from room temperature to 473 K in the presence of 13.33 kPa of hydrogen. Since the 2,6-lutidine preadsorbed sample was outgassed at 473 K, the acid sites under consideration are only strong acid sites that can retain 2,6-lutidine at the outgassing temperature of 473 K and below. As the temperature of hydrogen was increased, the intensity of the bands at 1605, 1585, 1460 and 1385 cm^{-1} corresponding to the Lewis acid sites decreased with a concomitant increase in the intensity of the bands at 1700, 1680,

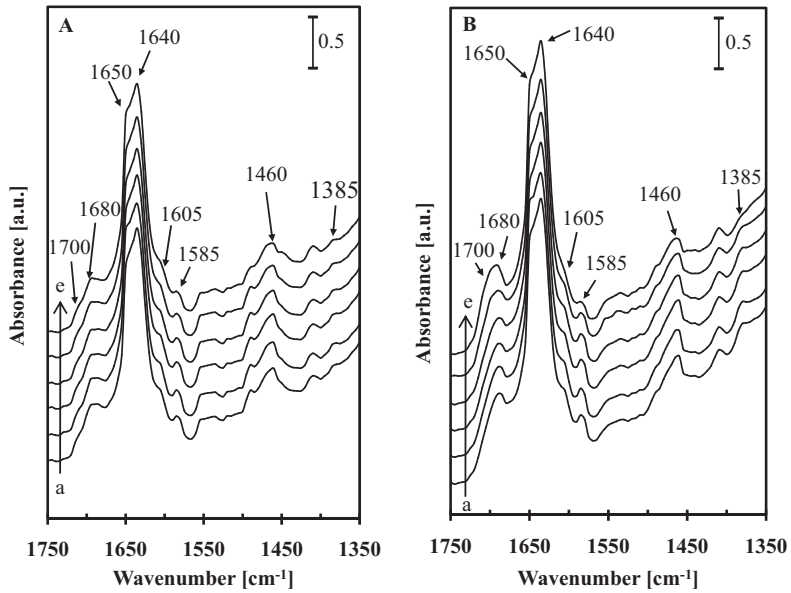

Fig. 11. IR spectra of 2,6-lutidine adsorbed on (A) Pt-HZSM5 and (B) Ir/Pt-HZSM5 when 2,6-lutidine-preadsorbed catalysts were heated in hydrogen at (b) room temperature, (c) 323 K, (d) 373 K, (e) 423 K and (f) 473 K. (a) Before exposure to hydrogen.

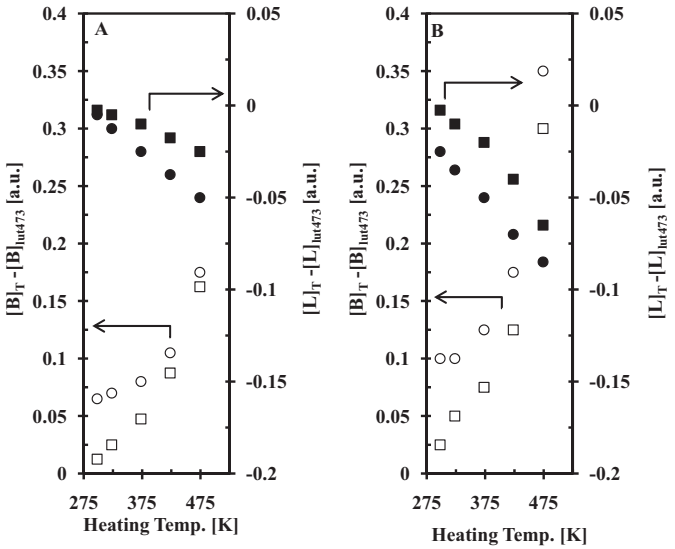

Fig. 12. The changes in Brönsted and Lewis acid sites of (A) Pt-HZSM5 and (B) Ir/Pr-HZSM5 when the catalysts were heated in the presence of 13.3 kPa hydrogen. (○) Brönsted acid sites at 1650 cm^{-1}, (□) Brönsted acid sites at 1640 cm^{-1}, (●) Lewis acid sites at 1605 cm^{-1}, (■) Lewis acid sites at 1585 cm^{-1}.

1650, and 1640 cm^{-1}, which are attributed to the peaks of 2,6-lutidine on Brönsted acid sites. Based on the concept of 'molecular hydrogenation-originated protonic acid sites', hydrogen molecules are dissociatively adsorbed on specific sites to form hydrogen atoms, followed by the release of electrons near to the cus metal cations forming protonic acid sites. Then, the electrons stabilized the cus metal cation as long as the 2,6-lutidine was protonated and interacted with extra-lattice or basic oxygen.

Fig. 11(B) shows the changes in the IR spectra as the 2,6-lutidine preadsorbed Ir/Pt-HZSM5 catalyst was heated from room temperature to 473 K in the presence of 13.33 kPa of hydrogen. The effect of hydrogen on the Ir/Pt-HZSM5 catalyst was essentially the same as that observed for the Pt-HZSM5 catalyst. Both catalysts have the ability to interchange the acidic characters of the Lewis and protonic acid sites when they are heated in the presence of molecular hydrogen. The elimination of Lewis acid sites and the formation of protonic acid sites as a function of temperature for both the Pt-HZSM5 and Ir/Pt-HZSM5 catalysts are clearly shown in Fig. 12. The conversion of Lewis acid sites to protonic acid sites was observed at room temperature for both catalysts. It should be noted, that the increase in the intensity of protonic acid sites is not similar to the decrease in the intensity of Lewis acid sites because of the different extinction coefficients for protonic and Lewis acid sites, as well as the ability of 2,6-lutidine to easily produce protonated species and weaker affinity for Lewis acid sites. Although both catalysts exhibited a similar phenomenon, Ir/Pt-HZSM5 formed more protonic acid sites than Pt-HZSM5 due to the increased number of stronger Lewis acid sites on Ir/Pt-HZSM5.

Although some differences among the catalysts exist, the interconversion of Lewis and protonic acid sites observed for Pt-HZSM5 and Ir/Pt-HZSM5 is essentially the same as that observed for $Pt/SO_4^{2-}–ZrO_2$ [2] and $Pt/WO_3–ZrO_2$ [55]. Pt species are a prerequisite for the formation of protonic acid sites from hydrogen molecules for $SO_4^{2-}–ZrO_2$ and HZSM5 but they are not required for $WO_3–ZrO_2$. The conversion of Lewis acid sites to protonic acid sites was appreciable at 473, 373, 323 and 323 K for $Pt/SO_4^{2-}–ZrO_2$, $Pt/WO_3–ZrO_2$, Pt-HZSM5 and Ir/Pt-HZSM5, respectively. We have also reported the interaction of molecular hydrogen on Pt/MoO_3 based on the quantitative analysis of the adsorption of hydrogen. Although the proposed mechanism for the interaction between molecular hydrogen and the catalyst is essentially the same with those of $SO_4^{2-}–ZrO_2$ and $WO_3–ZrO_2$, we suggested that the adsorption of hydrogen form a hydrogen molybdenum bronze on Pt/MoO_3 [6].

Table 1
Product distribution of *n*-pentane isomerization over Pt-HZSM5 and Ir/Pt-HZSM5 catalysts at 140 min time on stream.

Catalyst	Pt-HZSM5	Ir/Pt-HZSM5
Conversion [%]	73.1	68.4
Selectivity [%]		
$C_1–C_2$	7.4	2.8
$C_3–C_4$	22.2	19.3
iC_5	68.4	76.6
C_6^+	1.9	1.2

3.4. Isomerization

Fig. 13 shows the product distributions for *n*-pentane isomerization over the Pt-HZSM5 and Ir/Pt-HZSM5 catalysts at 573 K in a microcatalytic pulse reactor. The outlet consisted of $C_1–C_4$ cracking products, iso-pentane, residual *n*-pentane and higher hydrocarbons.

The addition of iridium to the Pt-HZSM5 catalyst has changed the selectivity for iso-pentane and $C_1–C_4$ cracking products in which the iso-pentane product increased from 68.4% to 76.6% and $C_1–C_4$ cracking products decreased from 29.6% to 22.1%. In addition, the conversion of *n*-pentane decreased by 4.7%. The product distribution of *n*-pentane isomerization at 140 min time on stream is listed in Table 1. Although it is not certain at present, strong bridged hydroxyl groups (Si(OH)Al) at 3610 cm^{-1} for both samples which shifted to a lower wavenumber due to the interaction with hydrogen in gas phase may act as active sites for both isomerization and cracking [63,64]. The enhancement in the iso-pentane selectivity of the Ir/Pt-HZSM5 catalyst may be caused by the interaction of iridium with lattice defects or extra-lattice oxygen resulting in an increased the number of strong Lewis and protonic acid sites from molecular hydrogen. Whereas, the suppression of $C_1–C_4$ cracking products may be caused by the inhibition of the formation of hydrogen bonding interactions from molecular hydrogen at 3680, 3600 and 3380 cm^{-1}.

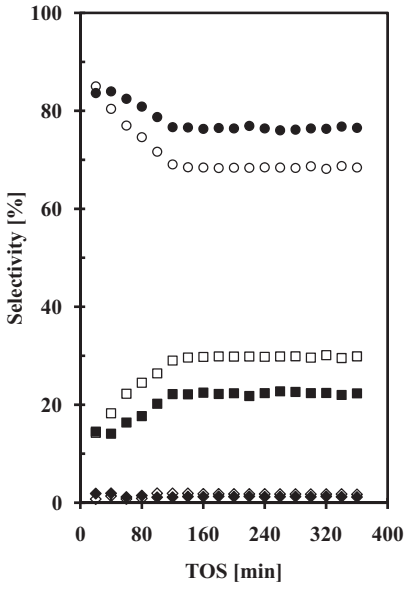

Fig. 13. Selectivity of (□,■) $C_1–C_4$; (○,●) iC_5; (◊, ♦) C_6^+ for isomerization of *n*-pentane at 573 K over Pt-HZSM5 and Ir/Pt-HZSM5 catalysts. White: Pt-HZSM5; black: Ir/Pt-HZSM5.

López et al. [65] reported the hydroisomerization of *n*-pentane over a Pt-HZSM5 catalyst in which the catalyst was prepared by wet impregnation of HZSM5 with a $Pt(NH_3)_4Cl_2$ solution. They found that incorporation of 0.5 wt% Pt in the HZSM5 catalyst resulted in a significant increase in *n*-pentane conversion. However, the cracking reaction is more favorable due to the unbalanced hydrogenation–dehydrogenation activity. Therefore, the introduction of second metal is necessary to increase the activity of Pt-HZSM5 and suppress the production of cracked products. Along this line, Aboul-Gheit et al. [28] studied the effect of iridium species on Pt-HZSM5 for *n*-hexane hydroconversion. They reported that the combination of platinum with iridium in the HZSM5 zeolite produces a more active catalyst compared to the monometallic Pt/HZSM5 catalyst, most probably due to the higher hydrogenation activity. Thus, the production of iso-hexane consequently increased from 65.1% to 67.9%.

The positive effect of iridium loaded on Pt-HZSM5 was also observed in this report in which the introduction of iridium to Pt-HZSM5 catalyst has increased the selectivity for iso-pentane and decreased the selectivity for cracking products. The increase in the selectivity for iso-pentane may be caused by the interaction of iridium with lattice defects or extra-lattice oxygen resulting in an increased the number of strong Lewis and protonic acid sites from molecular hydrogen. While, the decrease in the selectivity for C_1–C_4 cracking products may be caused by the bonding of iridium to perturbed silanol groups which inhibited the formation of hydrogen bonding interactions from molecular hydrogen at 3680, 3600 and 3380 cm^{-1}.

4. Conclusion

The study showed that iridium in the form of IrO_2 was bonded to perturbed silanol groups throughout the surrounding by lattice defects or extra-lattice oxygen, which stabilized the crystalline structure of HZSM5, leading to a more ordered framework structure and a higher surface area. The presence of iridium did not change the lattice structure of HZSM5 but slightly increased the number of Lewis and Brönsted acid sites and increased the number of protonic acid sites via hydrogen spillover phenomena as evidenced by 2,6-lutidine pre-adsorbed IR spectroscopy. The hydrogen IR study revealed that the presence of iridium inhibit the formation of hydroxyl group species from molecular hydrogen at 3380, 3600 and 3680 cm^{-1}.

In the presence of hydrogen in gas phase, strong bridged hydroxyl groups (Si(OH)Al) may act as active sites for both isomerization and cracking. The increase in the selectivity for iso-pentane of the Ir/Pt-HZSM5 catalyst may be caused by an increase in the acidity of the catalyst facilitating the formation of active protonic acid sites. Whereas, the decrease in the cracking products may be caused by the bonding of iridium to perturbed silanol groups of Pt-HZSM5 which inhibited the formation of hydroxyl groups from molecular hydrogen at 3680, 3600 and 3380 cm^{-1}.

Acknowledgments

This work was supported by The Ministry of Higher Education, Malaysia through the Fundamental Research Grant Scheme No. 78670 and the UTM Short Term Research Grant No. 77330. Our gratitude also goes to Universiti Malaysia Pahang for the award of Skim Fellowship Universiti Malaysia (Herma Dina Setiabudi) and the Hitachi Scholarship Foundation for the Gas Chromatograph Instruments Grant.

References

[1] F. Garin, S. Aeiyach, P. Legare, G. Maire, J. Catal. 77 (1982) 323–337.
[2] K. Ebitani, J. Konishi, H. Hattori, J. Catal. 130 (1991) 257–267.
[3] H. Sakagami, T. Ohno, N. Takahashi, T. Matsuda, J. Catal. 241 (2006) 296–303.
[4] S. Triwahyono, T. Yamada, H. Hattori, Appl. Catal. A: Gen. 250 (2003) 75–81.
[5] S. Triwahyono, A.A. Jalil, H. Hattori, J. Nat. Gas Chem. 16 (2007) 252–257.
[6] S. Triwahyono, A.A. Jalil, S.N. Timmiati, N.N. Ruslan, H. Hattori, Appl. Catal. A: Gen. 372 (2010) 103–107.
[7] A. Corma, D. Kumar, Stud. Surf. Sci. Catal. 117 (1998) 201–222.
[8] J. Weitkamp, P.A. Jacobs, J.A. Martens, Appl. Catal. 8 (1983) 123–141.
[9] K. Fujimoto, K. Maeda, K. Aimoto, Appl. Catal. A: Gen. 91 (1992) 81–86.
[10] P. Cañizares, A. de Lucas, J.L. Valverde, F. Dorado, Ind. Eng. Chem. Res. 36 (1997) 4797–4808.
[11] P.N. Kuznetsov, J. Catal. 218 (2003) 12–23.
[12] J.N. Kondo, S. Yang, Q. Zhu, S. Inagaki, K. Domen, J. Catal. 248 (2007) 53–59.
[13] C.S. Cundy, Chem. Rev. 103 (2003) 663–702.
[14] T. Inui, F. Okazumi, J. Catal. 90 (1984) 366–367.
[15] E. Iglesia, J.E. Baumgartner, G.L. Price, J. Catal. 134 (1992) 549–571.
[16] H. Kitagawa, Y. Sendoda, Y. Ono, J. Catal. 101 (1986) 12–18.
[17] J.A. Biscardi, E. Iglesia, J. Catal. 182 (1999) 117–128.
[18] J.A. Biscardi, G.D. Meitzner, E. Iglesia, J. Catal. 179 (1998) 192–202.
[19] S. Triwahyono, A.A. Jalil, M. Musthofa, Appl. Catal. A: Gen. 372 (2010) 90–93.
[20] H. Hattori, Stud. Surf. Sci. Catal. 77 (1993) 69–76.
[21] T. Shishido, H. Hatori, Appl. Catal. A: Gen. 146 (1996) 157–164.
[22] E. Blomsma, J.A. Martens, P.A. Jacobs, J. Catal. 165 (1997) 241–248.
[23] R.L.V. Mao, M.A. Saberi, Appl. Catal. A: Gen. 199 (2000) 99–107.
[24] Y.J. Huang, S.C. Fung, W.E. Gates, G.B. McVicker, J. Catal. 118 (1989) 192–202.
[25] J.H. Sinfelt, US Patent 3,953,368 (1976).
[26] M.J. Dees, V. Ponec, J. Catal. 115 (1989) 347–355.
[27] O.B. Yang, S.I. Woo, New frontiers in catalysis, in: L. Guczi, F. Solymosi, P. Tetenyi (Eds.), Proceeding of the 10th International Congress on Catalysis, vol. 75, Elsevier, New York, 1993, pp. 671–680.
[28] A.K. Aboul-Gheit, A.E. Awadallah, N.A.K. Aboul-Gheit, E.S.A. Solyman, M.A. Abdel-Aaty, Appl. Catal. A: Gen. 334 (2008) 304–310.
[29] S. Triwahyono, Z. Abdullah, A.A. Jalil, J. Nat. Gas Chem. 15 (2006) 247–252.
[30] A. Jentys, R.R. Mukti, H. Tanaka, J.A. Lercher, Microporous Mesoporous Mater. 90 (2006) 284–292.
[31] H.D. Setiabudi, S. Triwahyono, A.A. Jalil, N.H.N. Kamarudin, M.A.A. Aziz, J. Nat. Gas Chem. 20 (2011) 477–482.
[32] R. Moreno-Tost, E. Rodríguez Castellón, A. Jiménez-López, J. Mol. Catal. A: Chem. 248 (2006) 126–134.
[33] J. Burkhard, L.D. Schmidt, J. Catal. 116 (1989) 240–251.
[34] T.V. Voskobojnikov, E.S. Shpiro, H. Landmesser, N.I. Jaeger, G. Schulz-Ekloff, J. Mol. Catal. A: Chem. 104 (1996) 299–309.
[35] S.M. Cabral de Menezes, Y.L. Lam, K. Damodaram, M. Pruski, Microporous Mesoporous Mater. 95 (2006) 286–295.
[36] P. Praserthdram, S. Phatanasri, J. Rungsimanop, P. Kanchanawanichkun, J. Mol. Catal. A: Chem. 169 (2001) 113–126.
[37] C.A. Fyfe, G.C. Gobbi, G.J. Kennedy, J. Phys. Chem. 88 (1984) 3248–3253.
[38] J. Dědeček, S. Sklenak, C. Li, B. Winterlova, V. Gábová, J. Brus, M. Sierka, J. Sauer, J. Phys. Chem. C 113 (2009) 1447–1458.
[39] C.A. Fyfe, Y. Feng, H. Grondey, G.T. Kokotailo, H. Gies, Chem. Rev. 91 (1991) 1525–1543.
[40] W. Zhang, X. Bao, X. Guo, X. Wang, Catal. Lett. 60 (1999) 89–94.
[41] D. Ma, Y. Shu, X. Han, X. Liu, Y. Xu, X. Bao, J. Phys. Chem. B 105 (2001) 1786–1793.
[42] M.M.J. Treacy, J.B. Higgins, Collection of Simulated XRD Powder Patterns for Zeolites, 4th ed., Elsevier, New York, 2001.
[43] S.I. Zones, C.Y. Chen, A. Corma, M.T. Cheng, C.L. Kibby, I.Y. Chan, A.W. Burton, J. Catal. 250 (2007) 41–54.
[44] S. Zheng, A. Jentys, J.A. Lercher, J. Catal. 219 (2003) 310–319.
[45] J. Shi, D.J. Guo, Z. Wang, H.L. Li, J. Solid State Electrochem. 9 (2005) 634–638.
[46] T. Goto, J.R. Vargas, T. Hirai, Mater. Trans. JIM 40 (1999) 209–213.
[47] H. Li, M. Li, Y. Chu, H. Nie, Microporous Mesoporous Mater. 117 (2009) 635–639.
[48] J. Szanyi, M.T. Paffett, Microporous Mater. 7 (1996) 201–218.
[49] J.A. Lercher, A. Jentys, in: J. Cejka, H. van Bekkum, A. Corma, F. Schuth (Eds.), Introduction to Zeolite Science and Practise, 3rd revised ed., Elsevier, Amsterdam, 2007, p. 452.
[50] M. Mihaylov, E. Ivanova, F. Thibault-Starzyk, M. Daturi, L. Dimitrov, K. Hadjiivanov, J. Phys. Chem. B 110 (2006) 10383–10389.
[51] V.B. Kazansky, A.I. Serykh, B.G. Anderson, R.A.V. Santen, Catal. Lett. 88 (2003) 211–217.
[52] E. Babůrek, J. Nováková, Appl. Catal. A: Gen. 190 (2000) 241–251.
[53] G.N. Vayssilov, J.A. Lercher, N. Rösch, J. Phys. Chem. B 104 (2000) 8614–8623.
[54] V.B. Kazansky, J. Catal. 216 (2003) 192–202.
[55] S. Triwahyono, T. Yamada, H. Hattori, Appl. Catal. A: Gen. 242 (2003) 101–109.
[56] S. Triwahyono, H. Hattori, T. Yamada, Proceeding of 13th Annual Saudi-Japanese Catalyst Symposium, Dhahran, Saudi Arabia, 2003.
[57] A. Corma, C. Rodellas, V. Fornes, J. Catal. 88 (1984) 374–381.
[58] T. Armaroli, M. Bevilacque, M. Trombetta, A.G. Alejandre, J. Ramirez, G. Busca, Appl. Catal. A: Gen. 220 (2001) 181–190.
[59] C. Monterra, G. Cerrato, G. Meligrana, Langmuir 17 (2001) 7053–7060.
[60] L. Oliviero, A. Vimont, J.C. Lavalley, F.R. Sarria, M. Gaillard, F. Maugé, Phys. Chem. Chem. Phys. 7 (2005) 1861–1869.
[61] L. Li, F. Zhang, N. Guan, M. Richter, R. Fricke, Catal. Commun. 8 (2007) 583–588.
[62] D. Mao, W. Yang, J. Xia, B. Zhang, Q. Song, Q. Chen, J. Catal. 230 (2005) 140–149.
[63] T. Shishido, H. Hattori, J. Catal. 161 (1996) 194–197.
[64] S. Triwahyono, A.A. Jalil, R.R. Mukti, M. Musthofa, N.A.M. Razali, M.A.A. Aziz, Appl. Catal. A: Gen. 407 (2011) 91–99.
[65] C.M. López, Y. Guillén, L. García, L. Gómez, Á. Ramírez, Catal. Lett. 122 (2008) 267–273.